Combustion Science and Technology
Publication details, including instructions for authors and subscription information:
http://www.informaworld.com/smpp/title~content=t713456315

Combustion and deposit formation behavior on the fireside surfaces of a pulverized fuel boiler fired with a blend of coal and petroleum coke

S. Srikanth[a]; D. S. Rao[a]; Swapan K. Das[b]; B. Ravikumar[b]; K. Nandakumar[c]; R. Dhanuskodi[c]; P. Vijayan[c]
[a] Madras Centre, National Metallurgical Laboratory, Chennai, India [b] Materials Characterization Division, National Metallurgical Laboratory, Jamshedpur, India [c] Research & Development Section, Bharat Heavy Electricals, Ltd., Tiruchirappalli, India

Online publication date: 17 September 2010

To cite this Article Srikanth, S. , Rao, D. S. , Das, Swapan K. , Ravikumar, B. , Nandakumar, K. , Dhanuskodi, R. and Vijayan, P.(2003) 'Combustion and deposit formation behavior on the fireside surfaces of a pulverized fuel boiler fired with a blend of coal and petroleum coke', Combustion Science and Technology, 175: 9, 1625 — 1647
To link to this Article: DOI: 10.1080/00102200302371
URL: http://dx.doi.org/10.1080/00102200302371

Combust. Sci. and Tech., 175: 1625–1647, 2003

ISSN: 0010-2203 print / 1563-521X online
DOI: 10.1080/00102200390226562

Taylor & Francis
Taylor & Francis Group

COMBUSTION AND DEPOSIT FORMATION BEHAVIOR ON THE FIRESIDE SURFACES OF A PULVERIZED FUEL BOILER FIRED WITH A BLEND OF COAL AND PETROLEUM COKE

S. SRIKANTH* AND D. S. RAO

National Metallurgical Laboratory, Madras Centre,
Chennai, India

SWAPAN K. DAS AND B. RAVIKUMAR

Materials Characterization Division,
National Metallurgical Laboratory,
Jamshedpur, India

K. NANDAKUMAR, R. DHANUSKODI, AND P. VIJAYAN

Research & Development Section,
Bharat Heavy Electricals, Ltd.,
Tiruchirappalli, India

The thermochemistry of the combustion of a blend of coal and 5% petroleum coke was analyzed. Thermodynamic modeling and microscopic techniques were used to study the behavior of the inorganic constituents upon combustion of the blend of coal and petroleum coke. The chemical composition and phase constitution of the combustion products, as well as the deposits at several temperatures corresponding to those at the various parts of the boiler, were deduced by free-energy minimization. These results were compared with

Received 22 August 2002; accepted 3 April 2003.

The authors are thankful to the director of the National Metallurgical Laboratory and the management of Bharat Heavy Electricals, Ltd., Tiruchirappalli, for permission to publish this work.

*Address correspondence to s_srikanth_99@yahoo.com

actual results obtained from a commercial pulverized fuel boiler fired with coal and petroleum coke blend. The deposits on the fireside surfaces of the boiler tubes in the various parts (water walls, platen superheater, final superheater, economizer, and electrostatic precipitator) of the commercial pulverized fuel boiler fired with coal and 5% petroleum coke were characterized by particle size analysis, chemical analysis, x-ray diffraction, optical microscopy, and scanning electron microscopy. The combustion gas composition was measured using a portable on-line gas analyzer for N_2, O_2, CO_2, H_2O, CO, NO, and SO_2. The thermodynamically predicted compositions and phase constitutions for the gas phase as well as the condensed phases are in good agreement with the experimental results.

Keywords: coal, petroleum coke, deposit formation, deposit characterization, thermodynamic modeling

INTRODUCTION

Formation of deposits on heat transfer surfaces is one of the main problems encountered in a pulverized-coal–fired boiler. The formation of deposits not only lowers the heat transfer rates, resulting in frequent maintenance and unscheduled shutdowns, but may also increase the risk of fireside corrosion of the metal surfaces. The formation of deposits in coal-fired utility boilers is intricately related to the combustion and ash formation behavior of the coal being used. The microscopic characteristics of coal, such as the nature and amount of inorganic matter present, their association, particle size distribution, and physical and chemical transformations during combustion, govern ash formation and the subsequent deposition behavior.

Baxter (1992) summarized the various mechanisms for the formation of ash: vaporization and recondensation of volatile components (Flagan and Sarofim 1984; Quann et al., 1982), fragmentation of ash (Raask, 1985), convective transport of ash, structural disintegration (Flagan and Sarofim, 1984), shedding from the surface of chars during combustion (Allen and Mitchell, 1985; Helble and Sarofim, 1989, Quann et al., 1982) and coalescence of ash within a char particle (Baxter and Mitchell 1992; Raask, 1985). The transport of the particles to the heat transfer surface depends not only on the properties of the ash species but also on the process conditions in the boiler such as gas velocity, gas flow patterns, and temperature (Baxter, 1992). Volatile species and small particles ($<1\,\mu m$) are transported mainly by diffusion. Another mode of small particle transport results from a transport force produced due to a local

temperature gradient, which is termed "thermophoresis." Transport by thermophoresis occurs for particles of size less than 10 μm. Larger particles (>10 μm) are transported by inertial forces associated with gas flow. In addition, the eddy forces in the gas stream aid transport of particles of intermediate size range (5–10 μm). Based on these modes of mass transport, four major mechanisms of deposition have been reported in the literature (Baxter et al., 1991) (1) inertial impaction including eddy impaction and sticking, (2) thermophoresis, (3) condensation, and (4) chemical reaction.

Some models for fly ash formation have been reported in the literature (Baxter et al., 1991; Loehden et al., 1989). Loehden et al. (1989) developed a model for the prediction of size and composition distributions of fly ash from known information on coal mineral matter. Baxter and coworkers (1991) also developed a theoretical model capable of predicting the elemental composition of ash deposits formed in pulverized-coal boilers using the information on the boiler operating parameters, the nature and amount of inorganic matter in coal, and the location within the boiler. Neither of these models take into account the phase transformations in the mineral matter during combustion and they are also not capable of predicting the phase constitution of the ash/deposit at the different locations of the boiler. The physical and chemical transformations of specific minerals in coal, as well as the interactions of minerals within a coal particle, have been studied in several experiments (Baxter, 1990; Harding and Mai, 1990; Huffman et al. 1989; Srinivasachar and Boni, 1989; Srinivasachar, Helble & Boni, 1990; Srinivasachar, Helble, Boni et al., 1990). The transformation and deposition characteristics of pyrite (FeS_2) under pulverized-coal combustion conditions was examined by Srinivasachar, Helble and Boni (1990) using Mössbauer spectroscopy, scanning electron microscopy, and energy dispersive x-ray analysis. They observed that pyrite initially decomposed to form pyrrhotite, and the pyrrhotite subsequently melted to form an iron oxysulfide droplet. As the oxide content increases, magnetite crystallizes out of the melt and forms hematite at larger residence times. Srinivasachar, Helble, Boni et al. (1990) have also studied the behavior of excluded illite [$KAl_2(AlSi_3O_{10})(OH)_2$] grains in a carbon matrix. They observed that illite melts at temperatures above 1400 K and interacts with other minerals such as quartz, kaolinite, and pyrite. Baxter (1990) studied the evolution of particle size distributions for pyrite and quartz minerals in coal during combustion. It was observed that the

pyrite thermally decomposes to pyrrhotite and iron oxides and that two to three fragments are formed per original pyrite particle. For silica, a decrease in the average grain size by a factor of up to 5 was observed and there was no interaction between the silica and other inorganic species or the gas phase.

The objective of this study is to analyze the thermochemistry of combustion and study the deposition behavior of a subbituminous coal from Korba mines of Central India blended with petroleum coke and to correlate it with experimental results obtained from a commercial pulverized-fuel boiler. The other objective is to study the transformation behavior of the inorganic constituents in the fuel blend upon combustion. This information is useful for the determination of heat transfer rates across the boiler tubes in the boiler and for the analysis of the erosion and fireside corrosion behavior of metal surfaces.

EXPERIMENTAL

Combustion and deposit evaluation was carried out in a commercial pulverized-fuel boiler. The commercial pulverized-fuel boiler fired with a blend of subbituminous coal and 5% petroleum coke is in operation in one of the thermal power plants in India and was designed and commissioned by Bharat Heavy Electricals, Ltd., Tiruchirappalli. The petroleum coke used is from a refinery on the western coast of India. An illustrative sketch of the boiler is given in Figure 1. The process conditions, such as throughputs of fuel and air, flue gas inlet and outlet temperatures, the metal surface temperatures in the various sections of the boiler, and the specifications of the materials used in each section, are given in Table 1. On-line monitoring of gas composition (N_2, O_2, CO_2, H_2O, CO, NO, and SO_2) was carried out using a portable electrochemical analyzer. The boiler fired with coal and 5% petroleum coke blend was in operation continuously for more than a month prior to the collection of deposits. The average particle size distribution of the feed is given in Table 2. Deposits from the various locations (ash hopper, water walls, platen superheater, final superheater, economizer, electrostatic precipitator, and induced draft fan) of the boiler were collected during the boiler shutdown period. The deposits had accumulated over an 8-hour period, the time interval adopted for the soot-cleaning operations. The deposits were collected mainly from the front (windward) side of the boiler tubes, that is, in the direction of the flue gas flow.

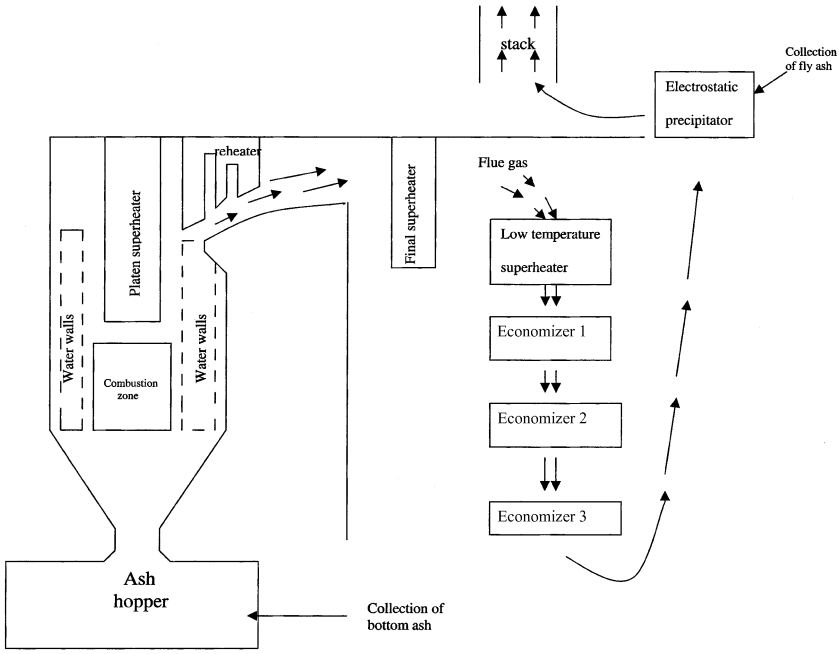

Figure 1. A schematic illustration of the commercial pulverized-fuel boiler.

Proximate and detailed ultimate analyses of both coal and petroleum coke were carried out. The petrology of the coal and the petroleum coke samples were also studied under an optical microscope (Leitz Orthoplan microscope) and in a scanning electron microscope (JEOL JSM 840 A) to identify the nature of the inorganic matter present and the size of the mineral particles. The ash as well as the deposit samples collected from the commercial pulverized-fuel boiler were subjected to particle size analysis, chemical analysis, optical microscopy, scanning electron microscopy, x-ray diffraction, and energy dispersive analysis (EDAX). The particle size analysis was carried out both on dry and wet modes in a CILAS (Model no. 1180) particle size analyzer. Chemical analyses were based mainly on atomic absorption spectrophotometry and complemented by EDAX attached to a scanning electron microscope. Microscopic studies were carried out via optical microscopy as well as scanning electron microscopy, in the backscatter as well as secondary electron imaging mode, to determine the morphology and compositional image of the deposits, the nature of minerals present, and the mineral

Table 1. Process conditions and material specification for the various components of the commercial pulverized-coal boiler

SI. No.	Boiler component	Flue gas temp Inlet/Outlet (°C)	Metal temperature (°C)	Material of construction ASME specification
1	Furnace waterwalls	1300°C/1175°C	450°C	SA210-Gr.C (C-0.35%, Mn-0.29–1.06%, S-0.058% max, P-0.048% max, Si-0.10%, rest Fe)
2	Platen superheater	1165°C/1058°C	500–550°C	SA213-T22 (C-0.15% max, Mn-0.3–0.6%, S-0.3% max, P-0.3% max, Si-0.5% max, Cr-1.9–2.6%, Mo-0.87–1.13%, rest Fe)
3	Reheater	845°C/1058°C	350–550°C	SA213-T22
4	Final superheater	815°C/780°C	520–560°C	SA213-T22
5	Low-temperature superheater	760°C/560°C	480–490°C	SA213-T11 (C-0.15% max, Mn-0.3–0.6%, P-0.30% max, S-0.30% max, Si-0.5–1.0%, Cr-1.0–1.5%, Mo-0.44–0.65%)
6	Economizer	360°C/340°C	350°C	SA210-Gr.C
7	Electrostatic precipitator	160°C/150°C		

Input rate of 95% coal + 5% petroleum coke blend: 81.4 tons/hr. Input rate of air: 533.6 tons/hr.

particle size. Mineral particle size measurement in the petrological microscope was carried out by standardizing the eyepiece scale in the microscope with that of a standard thin glass slide microscale. Sizes up to

Table 2. Particle size distribution of the fuel (95% coal + 5% petcoke) used in the commercial boiler

Mesh aperture size (μm)	Percent distribution
+ 50 mesh (>300 μm)	0.30
+ 100 mesh (>150 μm)	1.70
+ 200 mesh (>75 μm)	20.10
−200 mesh (<75 μm)	77.90

1 μm (scale of 2 mm divided into 20×10 divisions) can be measured accurately using this technique.

EQUILIBRIUM THERMODYNAMIC CALCULATIONS

The equilibrium flue gas composition upon combustion, as well as that of the various condensed phases, was deduced at various temperatures (corresponding to those in the various portions of the boiler) using a free-energy minimization technique incorporated in the FactSage software (version 5.1) (Thermfact, 2000). The thermodynamic data of all the relevant phases for the free-energy minimization were taken from the thermodynamic database provided in the FactSage software. The relevant solution phases were carefully selected based on the concentration range in which they successfully describe the thermodynamic properties. These include the slag phase; chloride, sulfate, and carbonate salt phases (solid and liquid); corundum and olivine solid solution phases; and so on.

RESULTS

The proximate and ultimate analyses of the coal and petroleum coke are given in Table 3. The optical micrographs of the coal sample are given in Figure 2 and the corresponding backscattered and secondary electron images taken in the SEM are shown in Figure 3. The micrograph of the coal sample shows the presence of coal lithotypes (vitrain, clarain, durain, and fusain), clay, quartz (SiO_2), and pyrite (FeS_2). The clay is revealed as elongated grains (30–100 μm size), whereas the quartz is present as sub-rounded or irregular-shaped grains (20–100 μm) within them. The silicates contain specks of pyrite (1–5 μm) as inclusions. Occasionally, the pyrite is also observed as clots/bunches. The scanning electron images of the polished petroleum coke sample indicate that it is fully amorphous and does not reveal any mineral matter.

The measured gas composition upon combustion of coal and 5% petroleum coke blend is given in Table 4 in comparison to the thermodynamically calculated values. It is seen that there is good agreement between the predicted and actual gas composition, except for NO, indicating attainment of equilibrium for the gas phase. The chemical composition of the deposits corresponding to the firing of a blend of coal and 5% petroleum coke collected from the various portions of the boiler is summarized in Table 5. It is observed that the deposit composition

Table 3. Proximate and ultimate analysis of coal and petroleum coke

	Coal (wt%)	Petroleum coke (wt%)
Moisture	4.40	0.40
Volatile Matter	18.04	12.81
Ash	35.80	1.80
Carbon	41.2	77.99
Hydrogen	2.34	3.35
Sulfur	0.56	7.00
Nitrogen	0.80	0.87
Chlorine	0.01	0.01
Oxygen (by difference)	14.92	8.59
SiO_2	23.70	1.18
Al_2O_3	7.20	0.117
TiO_2	0.18	0.009
Fe_2O_3	2.68	0.166
CaO	1.25	0.133
MgO	0.54	0.018
Na_2O	0.18	0.162
K_2O	0.036	0.002
P_2O_5	Nil	0.009

more or less resembles the coal ash composition and there is not much variation in the chemical composition of the deposits in the various portions of the boiler. This indicates that the deposit formation has predominantly been by way of the inertial mechanism in all parts of the boiler. There is no evidence of any gas-phase condensation in any of the parts of the boiler except in the electrostatic precipitator, wherein some moisture condensation is observed.

The particle size distribution of the deposits collected from the various locations of the boiler is depicted in Figure 4. It is seen that the particle size distribution in the ash hopper and water wall is spread out in the range of 0–250 μm and to a limited extent is similar to the particle size distribution of the feed. The ash hopper further contained sintered slag samples ranging from 100 μm to 1 cm, which were sieved out (> 0.085 mm) prior to carrying out the particle size analysis. On the other hand, the particle sizes of the deposits in the superheaters, economizer, and electrostatic precipitator were much finer and in a very narrow range of 0–50 μm. It is obvious that the particle size distribution in these deposits is very different from the feed size distribution.

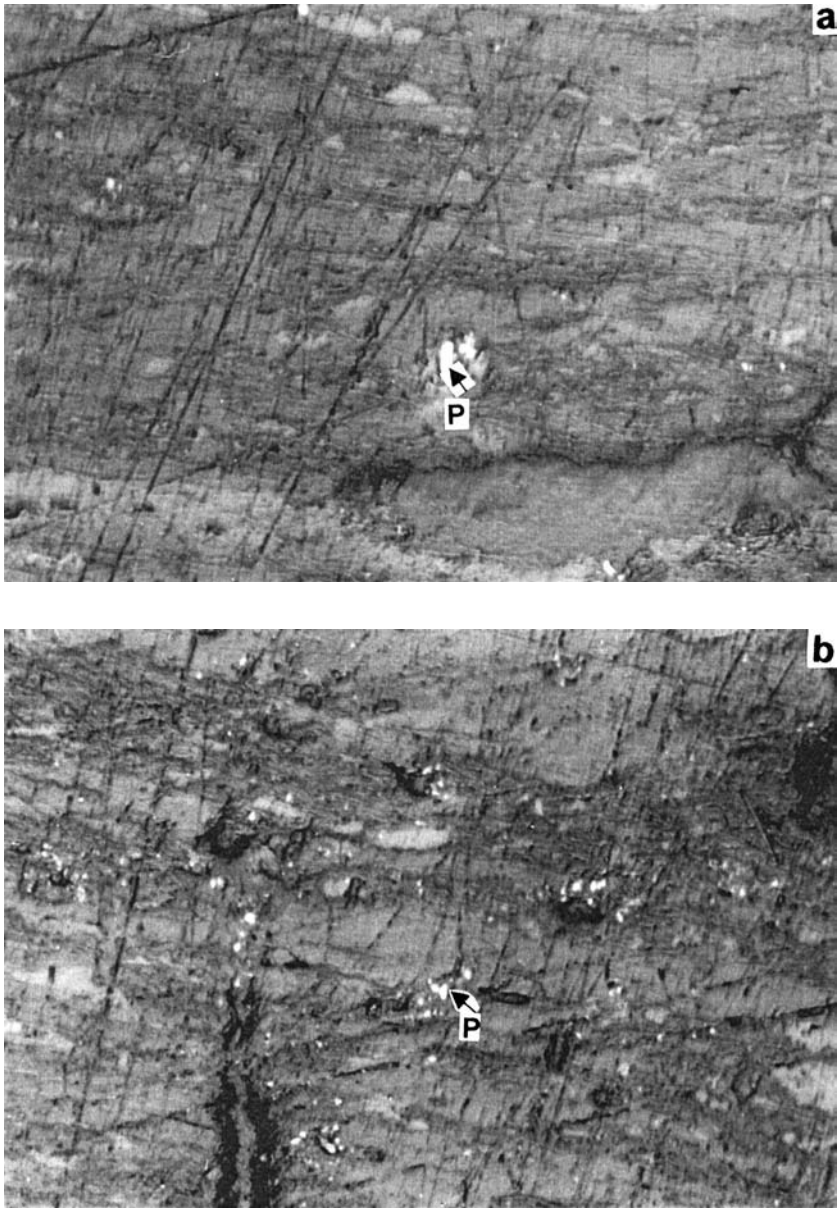

Figure 2. Optical micrographs of the coal sample (P indicates pyrite); scale 1 cm = 65 μm.

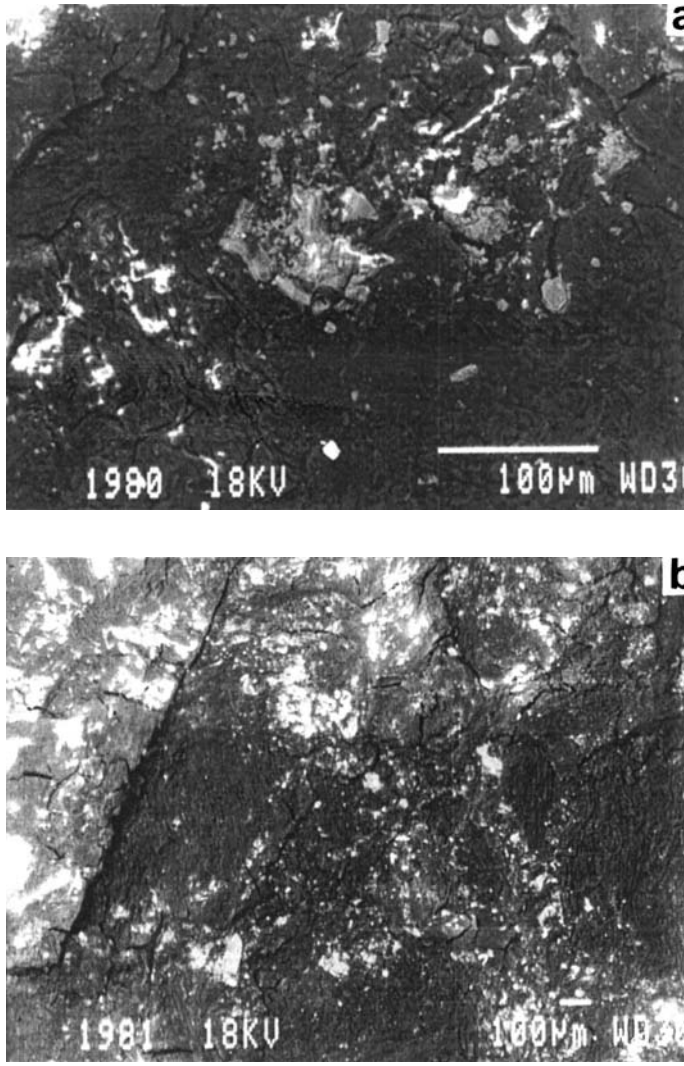

Figure 3. Backscattered electron images of the coal sample showing atomic number contrast. The white patches are pyrite and the gray patches are silicates.

The stereomicrographs of the ash hopper deposit and the water wall deposit are shown in Figures 5 and 6, respectively. The stereomicrograph of the separated (sieved) slag particles is also shown in Figure 5. The water wall deposit comprises coarse and fine slag particles along with quartz,

Table 4. Comparison of the thermodynamically predicted and actual gas compositions for the combustion of coal and 5% petroleum coke blend

	Composition (vol%)	
Gas species	Thermodynamic prediction	Experimental[a]
N_2	74.19	70.0–75.0
CO_2	14.92	13.0–15.5
H_2O	5.88	10.0–12.0
O_2	3.80	3.5–5.25
CO	0.0116	0.001–0.021
SO_2	0.1141	0.031–0.075
NO	0.1672	0.03–0.045

[a]Range of compositions recorded over a period of time.

mullite ($Al_6Si_2O_{13}$), sillimanite (Al_2SiO_5), and hematite (α-Fe_2O_3). The fine slag particles are revealed as rounded to subrounded particles. The quartz particles appear as cryptocrystalline unevenly broken grains, transparent and colorless, in the size range 5–70 μm. The mullite particles are revealed as white rods, rectangular plates/scales, and elongated prismatic crystals/plates in the size range 20–150 μm. The sillimanite phase appears as needle or acicular-shaped crystals in the size range 10–50 μm. The hematite occurs as globules, nodules, or sometimes as aggregates of nodules in the size range 20–80 μm and occasionally up to 150 μm. The amount of slag is estimated to be in the range of 60–70%, followed by quartz, mullite, sillimanite, and hematite phases in order of abundance. The water wall deposit also contains the slag phase, quartz, mullite, and hematite, and their morphology is the same as that observed for the ash hopper deposit. However, the relative abundance of these phases, as well as the mineral particle sizes, varies. The slag phase in this case is estimated to be around 20–30% in the size range of 100–400 μm globules; the quartz particles are in the size range of 5–100 μm, mullite in the size range 20–100 μm, hematite in the size range of 20–80 μm, and traces of sillimanite in the range 5–20 μm.

The photomicrographs of the platen superheater, final superheater, economizer, and electrostatic precipitator deposits are depicted in Figures 7 (a)–(d), respectively. The features in all these micrographs are very similar and reveal the presence of quartz, mullite, and hematite in

Table 5. Predicted and experimental compositions of the deposits for the combustion of 95% coal + 5% petroleum coke blend in the various parts of the boiler

	Experimental (AAS & EDS) and predicted chemical composition (thermodynamic modeling)—weight percent										
Location in the boiler	SiO_2	K_2O	CaO	MgO	Al_2O_3	Na_2O	Fe_2O_3	SO_3	TiO_2	Cl (ppm)	H_2O
Ash hopper											
Actual	62.9	0.80	2.50	0.70	18.60	0.60	12.10	—	0.6	—	—
Predicted	66.2	0.10	3.70	1.47	19.45	0.92	7.59	Nil	0.5	Nil	Nil
Furnace water walls											
Actual	63.80	0.82	0.93	0.41	22.56	0.05	8.08	2.58	1.4	80	Nil
Predicted	66.25	0.10	3.70	1.48	19.45	0.93	7.59	Nil	0.5	Nil	Nil
Platten superheater											
Actual	59.89	0.96	3.38	0.51	22.70	0.06	8.30	3.35	1.19	Nil	0.18
Predicted	66.26	0.10	3.70	1.48	19.44	0.93	7.59	Nil	0.5	Nil	Nil
Final superheater											
Actual	63.66	0.98	0.38	0.48	22.62	0.09	5.04	5.5	1.19	65	0.06
Predicted	62.93	0.09	3.57	1.40	18.47	0.88	7.21	5.02	0.47	Nil	Nil
Economizer											
Actual	62.06	1.04	0.82	0.58	19.45	0.08	6.09	6.25	1.07	115	3.0
Predicted	62.23	0.09	3.47	1.38	18.26	0.87	7.13	6.07	0.47	Nil	Nil
Electrostatic precipitator											
Actual	60.55	1.00	1.10	0.63	19.65	0.07	5.85	5.48	1.08	115	3.90
Predicted	59.97	0.09	3.35	1.34	17.60	0.84	6.87	5.85	0.45	125	3.62

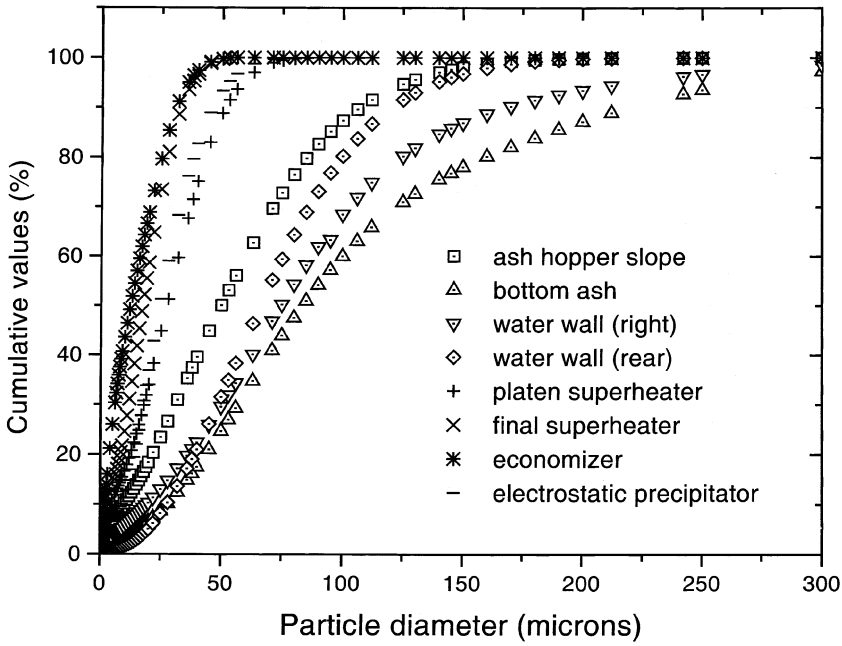

Figure 4. Particle size distributions in the deposits collected from the various locations in the boiler.

decreasing abundance and traces of slag. In general, in these deposits, the quartz mineral particles are in the size range 5–50 μm, the mullite particles are in the size range 10–50 μm, and hematite particles are in the size range 5–40 μm. The SEM photomicrographs in the backscattered electron imaging mode depicting the composition image of deposits from the various parts of boiler are delineated in Figures 8 (*a*)–(*f*), respectively. The SEM results substantiate the observations made in the optical micrographs, that is, the presence of large amounts of slag, some quartz, sillimanite, and traces of mullite in the high-temperature deposits and the presence of quartz, mullite, and hematite in varying proportions at low temperatures. Furthermore, it is seen that the size of the mineral particles becomes progressively lower as they travel from the water wall to the electrostatic precipitator.

The x-ray diffraction pattern of the deposits is shown in Figure 9 and the phases present in the various deposits are summarized in Table 6. All the deposits show the presence of crystalline quartz, mullite, and

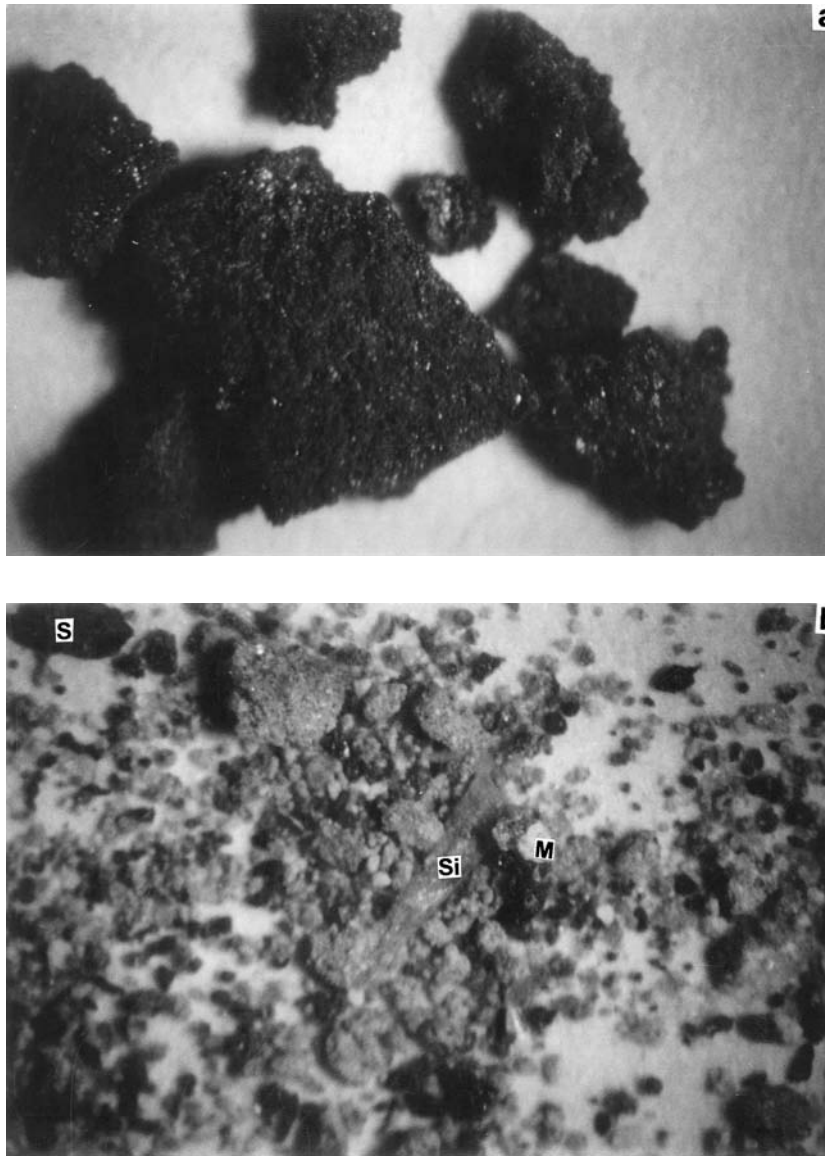

Figure 5. Stereomicrographs of the ash hopper deposit: (a) picture of the coarse slag sample; the white spots within the slag are mullite; (b) general view of the ash hopper deposit at $12\times$ (Si indicates sillimanite and M is mullite).

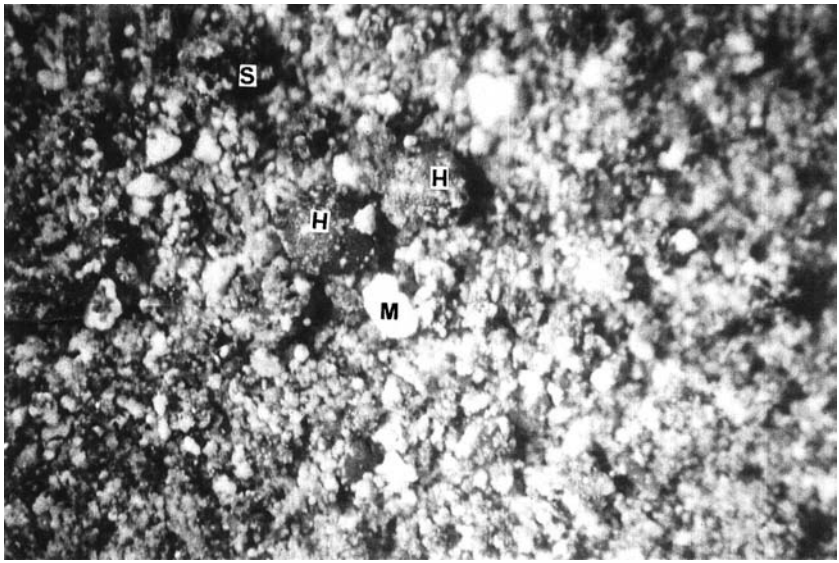

Figure 6. Stereomicrographs of the water wall deposit at 12× (M stands for mullite, H for hematite, and S for slag particles).

hematite. In addition, the water wall deposit shows the presence of small amounts of sillimanite. The main drawback of x-ray diffraction is that amorphous phases such as the slag phase and presence of minor phases (< 3 vol%) cannot be detected.

Thermodynamic calculations were carried out to determine the ash composition as a function of combustion temperature for the firing of the coal and 5% petroleum coke mixture. The calculations indicate that the ash will exist completely as liquid slag at temperatures of combustion above 1400 °C. Below this temperature, solid crystalline phases such as corundum, tridymite, and mullite are predicted to coexist with the slag phase. However, in actual practice, because the residence time of the ash particles in the combustion zone is very small, only partial slag formation results even at temperatures higher than 1400 °C. The ash fusion temperature determined from laboratory experiments was found to be 1450 °C for the mixture of coal with 5% petroleum coke. The various phases at equilibrium, their amounts in weight percent, and their equilibrium composition at the different temperatures corresponding to the various parts of the boiler determined through the free-energy

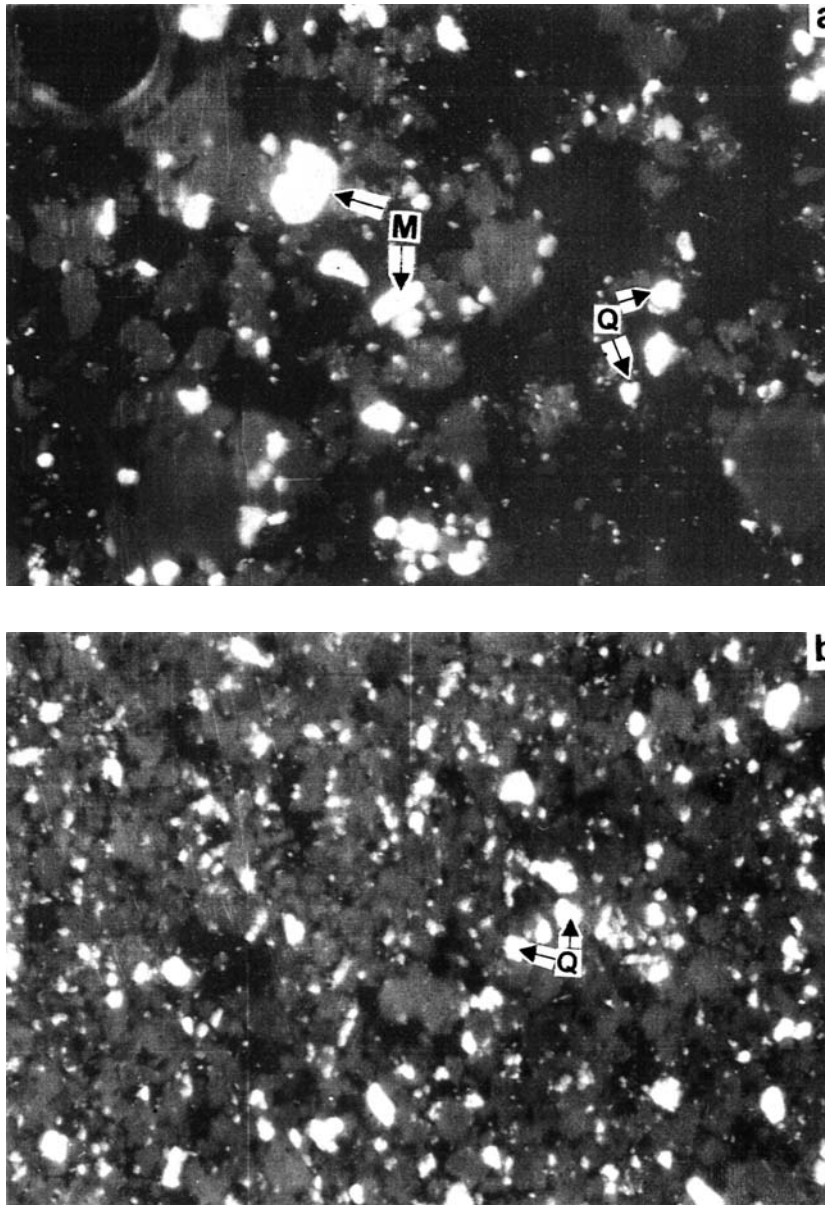

Figure 7. Optical micrographs of the deposits from (a) platen superheater, (b) final superheater, (c) economizer, and (d) electrostatic precipitator. Scale: 1 cm = 65 μm (Q indicates quartz and M indicates mullite).

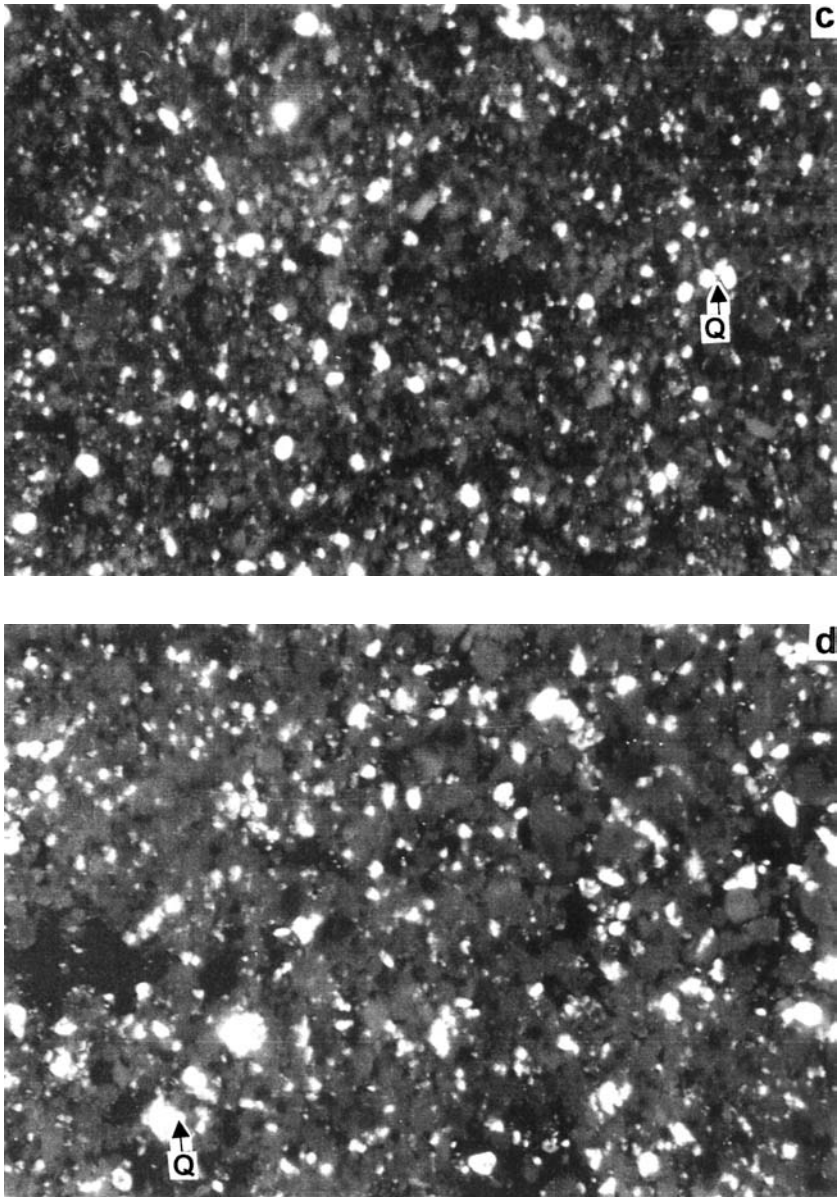

Figure 7. (*Continued*).

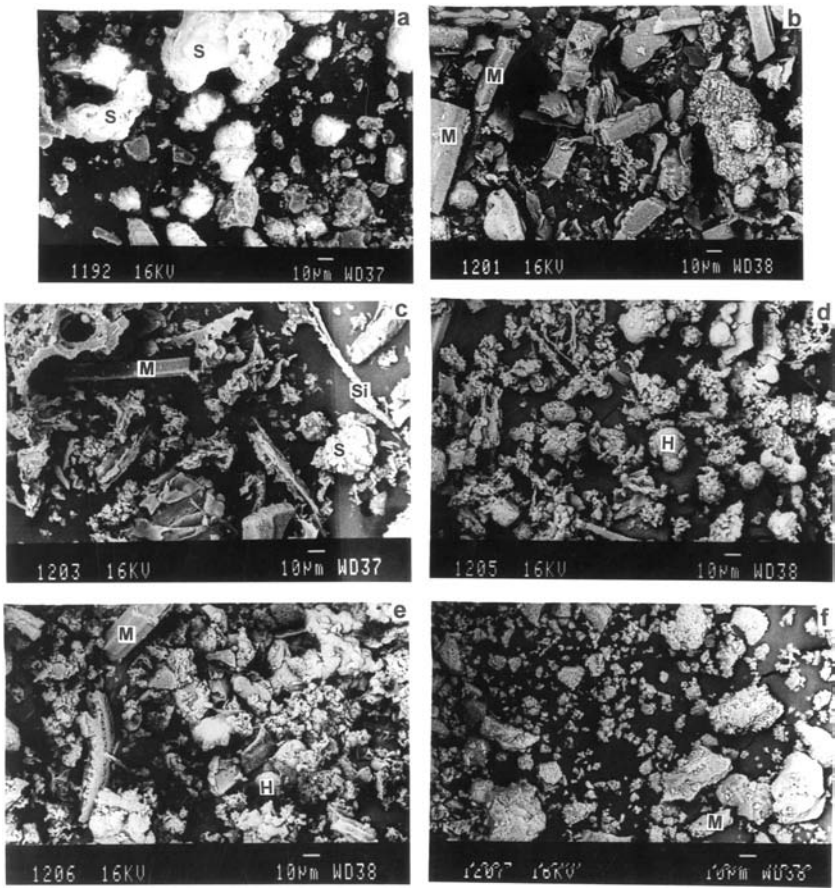

Figure 8. SEM photographs in the backscattered electron imaging mode giving the morphology of the deposits from (a) ash hopper, (b) water walls, (c) platen superheater, (d) final superheater, (e) economizer, and (f) electrostatic precipitator.

minimization procedure are also listed in Table 6. The metal surface temperature is generally lower than the flue gas temperature at the same position and a temperature gradient exists across the deposits. Furthermore, the flue gas temperature at the inlet and outlet are different. However, for computing the equilibrium phases by free-energy minimization, it was assumed that the deposit temperature at the surface corresponds to the flue gas temperature. The mean value of the inlet and outlet temperatures was used for the calculations.

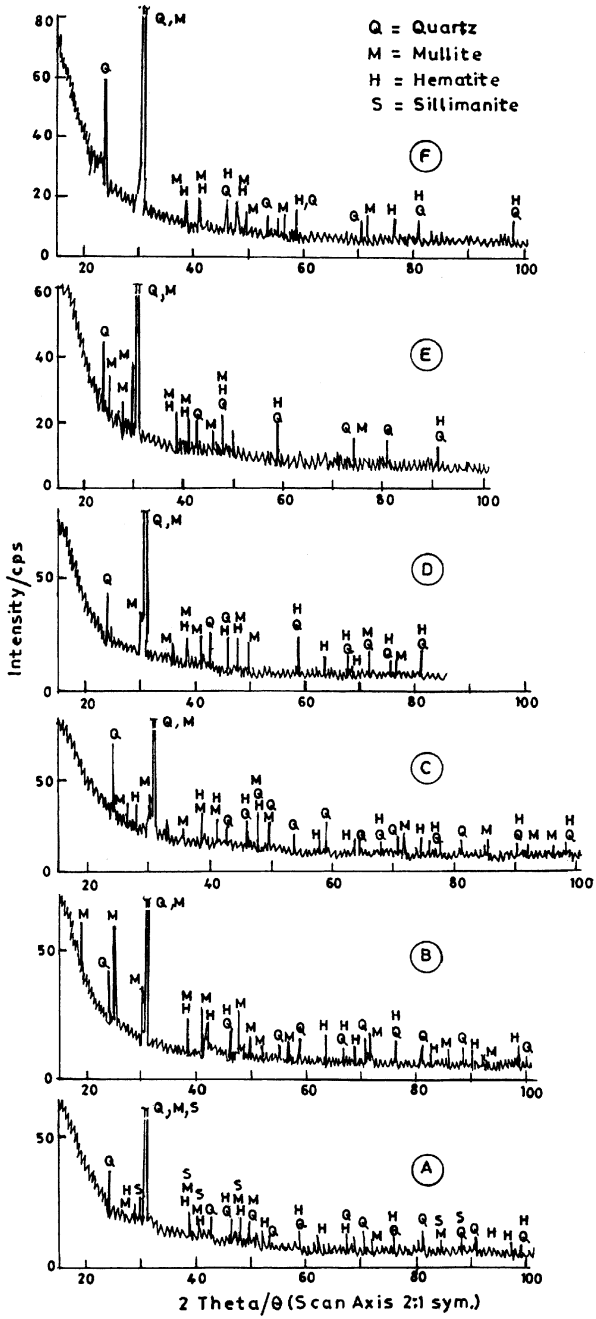

Figure 9. X-ray diffractograms of the deposits from (a) ash hopper, (b) water walls, (c) platen superheater, (d) final superheater, (e) economizer, and (f) electrostatic precipitator.

Table 6. Comparison of the experimental and equilibrium phase constitution of the deposits in the various locations of the boiler

Location in the boiler	Phase constitution (weight percent)	
	Experimental (XRD & SEM)	Equilibrium (thermodynamic modeling)
Ash hopper	Slag, quartz (SiO_2), mullite ($Al_6Si_2O_{13}$), hematite (α-Fe_2O_3), sillimanite (Al_2SiO_5)	Slag-72% (X_{SiO2}-0.77, X_{Al2O3}-0.12, X_{CaO}-0.059, X_{MgO}-0.033, X_{Na2O}-0.013, X_{TiO2}-0.006), tridymite (SiO2)-12.66%, corundum soln - 8.33% (X_{Fe2O3}-0.87, X_{Al2O3}-0.13), mullite-7.19%
Furnace water walls	Quartz (SiO_2), mullite ($Al_6Si_2O_{13}$), hematite (α-Fe_2O_3)	Slag-57% (X_{SiO2}-0.74, X_{Al2O3}-0.12, X_{CaO}-0.074, X_{MgO}-0.041, X_{Na2O}-0.017, X_{TiO2}-0.007), tridymite (SiO2)-24.06%, corundum soln - 8.3% (X_{Fe2O3}-0.87, X_{Al2O3}-0.13), mullite-10.58%
Platten superheater	Quartz (SiO_2), mullite ($Al_6Si_2O_{13}$) hematite (α-Fe_2O_3)	Slag-19% (X_{SiO2}-0.73, X_{Al2O3}-0.11, X_{CaO}-0.05, X_{MgO}-0.034, X_{Na2O}-0.051, X_{TiO2}-0.021), tridymite (SiO2)-40.33%, corundum soln - 8.21% (X_{Fe2O3}-0.89, X_{Al2O3}-0.11), mullite-10.3%, anorthite ($CaAl_2Si_2O_8$)-14.29%, cordierite ($Mg_2Al_4Si_5O_{18}$)-7.82%
Final superheater	Quartz (SiO_2), mullite ($Al_6Si_2O_{13}$) hematite (α-Fe_2O_3)	Quartz (SiO_2)-47.26%, corundum soln - 7.64% (X_{Fe2O3}-0.915, X_{Al2O3}-0.084), mullite - 18.04%, cordierite ($Mg_2Al_4Si_5O_{18}$)-10.16%, $NaAlSi_3O_8$-7.44%, rutile (TiO_2)-0.48%, leucite ($KAlSi_2O_6$)—0.44%, solid salt soln-8.55% (X_{CaSO4}—0.999, X_{MgSO4}-0.001)
Economizer	Quartz (SiO_2), mullite ($Al_6Si_2O_{13}$) hematite (α-Fe_2O_3)	Quartz (SiO_2)-48.01%, corundum soln - 7.13% (X_{Fe2O3}-1.0), cordierite ($Mg_2Al_4Si_5O_{18}$)-10.05%, $NaAlSi_3O_8$-0.1%, rutile (TiO_2)-0.47%, andalusite ($KAlSi_2O_5$)-23.26%, solid salt soln-10.40% (X_{CaSO4}—0.82, X_{Na2SO4}-0.18)
Electrostatic precipitator	Quartz (SiO_2), mullite ($Al_6Si_2O_{13}$), hematite (α-Fe_2O_3)	

DISCUSSION

It is clear that the original minerals present in the coal undergo several transformations upon combustion. Of the phases that have been observed in the deposits, only quartz was present originally in the coal sample. Other than slag, mullite and sillimanite form from the clay, and the hematite phase forms from the pyrite present in the coal. As suggested by Baxter (1990), it appears that the quartz liberated on combustion remains inert and does not interact with the other liberated inorganic species. However, the reduction in the quartz particle size upon combustion in the present case is lower than that observed in the studies of Baxter (1990). The transformation of pyrite under pulverized-coal combustion conditions were examined by Srinivasachar, Helble and Boni (1990). They observed that pyrite initially decomposed to form pyrrhotite and the pyrrhotite subsequently melted to form an iron oxysulfide droplet. As the oxide content increases, magnetite crystallizes out of the melt and forms hematite at larger residence times. The transformation of pyrite to hematite is observed in the current study. It is well known that when any clay (especially kaolinite type) is heated beyond 800 °C, it forms mullite and crystoballite (Deer et al., 1983). The crystoballite subsequently transforms to quartz at lower temperatures.

X-ray diffraction and microscopic investigations of the different deposits do not reveal any further transformations of the quartz, mullite, and hematite mineral particles during their passage along with the flue gas from the combustion zone to the electrostatic precipitator. However, the amount of slag or amorphous phase observed at lower temperatures (< 1000 °C) in the deposit samples is very little. This is mainly because the slag particles are larger and heavier and they are collected either in the ash hopper or deposited on the water walls and are not carried along with the flue gas. The minor amounts of slag that are carried along with the flue gas appear to crystallize at lower temperatures. Scanning electron microscopic studies as well as petrological studies on the deposits also indicate a progressive increase in the relative amounts of quartz and mullite in the deposits at lower temperature, supporting partial crystallization from the slag phase. The mineral particle sizes of quartz, mullite, and hematite become progressively lower from water walls to platen superheater to final superheater to economizer down to the electrostatic precipitator. This may be caused by abrasion within the gas phase as well as fragmentation due to impaction with the metal surfaces.

Thermodynamic calculations indicate that the amount and composition of slag in the ash and, consequently, the viscosity of the ash particles depend strongly on the temperature of combustion. The transport of the ash particles to the heat transfer surfaces and sintering characteristics of the deposits, as well as adhesion and growth of ash deposits on metal surfaces, depend on the composition and phase constitution of the ash formed on combustion. The thermodynamically predicted compositions and phase constitution of the deposits in the various locations of the boiler are in reasonable agreement with the experimental results, especially for the deposits in high-temperature zones. The thermodynamically predicted formation of the more complex phases, such as anorthite, cordierite, andalusite, and so on at lower temperatures in the superheater and economizer zones is not actually realized because of the nonattainment of equilibrium at lower temperatures.

REFERENCES

Allen, R.M. and Mitchell, R.E. (1985) Proceedings of the 1985 International Conference on Coal Science, The International Energy Agency, pp. 401–404.

Baxter, L.L. (1990) The evolution of mineral particle size distributions during early stages of coal combustion. *Prog. Energy Combust. Sci.*, **16**, 261–266.

Baxter, L.L. (1992) Char fragmentation and fly ash formation during pulverized-coal combustion. *Combust. Flame*, **90**, 174–184.

Baxter, L.L., Abbott, M.F., and Douglas, R.E. (1991) Dependence of elemental ash deposit composition on coal ash chemistry and combustor environment. In S.A. Benson, (Ed.) *Inorganic Transformations and Ash Deposition During Combustion*, American Society of Mechanical Engineers, Palm Coast, FL, pp. 679–698.

Baxter, L.L. and Mitchell, R.E. (1992) The release of iron during the combustion of Illinois 6 coal. *Combust. Flame*, **88**, 1–14.

Deer, W.A., Howail, R.A., and Zussman, J. (1983) *An Introduction to the Rock Forming Minerals*, ELBS and Longman Publications, Harlow, Essex, England, UK.

Flagan, R.C. and Sarofim, A.F. (1984) Comments to the article by W.T. Reid "The relation of mineral composition to slagging, fouling and erosion during and after combustion". *Prog. Energy Combust. Sci.*, **10**, 159–175.

Harding, N.S. and Mai, M.C. (1990) Elemental partitioning during pilot-scale combustion tests—Effects on ash deposition. In R.W. Bryers, and K.S. Vorres, (Eds.) *Mineral Matter and Ash Deposition from Coal*, Engineering Trustees Inc., New York, pp. 375–399.

Helble, J.J. and Sarofim, A.F. (1989) Factors determining the primary particle size of flame generated inorganic aerosols. *J. Colloid Interf. Sci.*, **128**, 348–262.

Huffman, G.P., Huggins, F.E., Levasseur, A.A., Chow, O., Srinivasachar, S., and Mehta, A.K. (1989) Investigations of the transformations of pyrite in a drop tube furnace. *Fuel*, **68**, 485–490.

Loehden, D., Malsh, P.M., Sayre, A.N., Beer, J.M., and Sarofim, A.F. (1989) Generation and deposition of fly ash in the combustion of pulverized coal. *J. Inst. Energy*, 62(451), 119–127.

Quann, R.J., Nevile, M., Janghorbani, M., Mims, C.A., and Sarofim, A.F. (1982) Mineral matter and trace element vaporization in laboratory pulverized coal combustion system. *Environ. Sci. Technol.*, **16**, 776–781.

Raask, E. (1985) *Mineral Impurities in Coal Combustion*, Hemisphere, New York.

Srinivasachar, S. and Boni, A. (1989) A kinetic model for pyrite transformations in a combustion environment. *Fuel*, **68**, 829–840.

Srinivasachar, S., Helble, J.J., and Boni A.A. (1990) Mineral bahavior during coal combustion 1. Pyrite transformations. *Prog. Energy Combust. Sci.*, **16**, 281–292.

Srinivasachar, S., Helble, J.J., Boni, A.A., Shah, N., Huffman, G.P., and Huggins, F.E. (1990) Mineral behavior during coal combustion 2. Illite transformations. *Prog. Energy Combust. Sci.*, **16**, 293–302.

Thermfact (2000) FactSage Programs and Databases Version 5.1 Thermfact Ltd., Mount Royal, Quebec, Canada.